Multi-Modular Wide-Band Capturing Nanohybrids: Role of Carbon Nanotubes in Slowing Charge Recombination in Supramolecular C_{60}-BisstyrylBODIPY-(Zinc Porphyrin)$_2$ Donor-Acceptor *Molecular Cleft*

Shahrzad Kazemi,[a] Ajyal Z. Alsaleh,[a,c] Paul A. Karr,[b] and Francis D'Souza*[,a]

[a]Department of Chemistry, University of North Texas, 1155 Union Circle, #305070, Denton, TX 76203-5017, United States

[b]Department of Physical Sciences and Mathematics Wayne State College, 1111 Main Street, Wayne, Nebraska, 68787, United States

[c]Current address: Imam Abdulrahman bin Faisal University, Dammam, 34212, Saudi Arabia.

ABSTRACT: The importance of diameter-sorted single-wall carbon nanotubes (SWCNTs) non-covalently bound to a donor-acceptor *molecular cleft*, **1**, in prolonging the lifetime of charge-separated states is successfully demonstrated. For this, using a multi-step synthetic procedure, a wide-band capturing, multi-modular, C_{60}-bisstyrylBODIPY-(zinc porphyrin)$_2$, *molecular cleft* **1**, was newly synthesized and shown to bind diameter sorted SWCNTs. The *molecular cleft* and its supramolecular assemblies were characterized by a suite of physico-chemical techniques. Free-energy calculations suggested that both the (6,5) and (7,6) SWCNTs bound to **1** act as hole acceptors during the photo-induced sequential electron transfer events. Consequently, selective excitation of **1** in **1**:SWCNT hybrids revealed a two-step electron transfer leading to the formation of charge-separated states. Due to the distal separation of the cation and anion radical species within the supramolecules, improved lifetimes of the charge-separated states could be achieved. The present supramolecular strategy of improving charge separation involving SWCNTs and donor-acceptor *molecular cleft* highlights the potential application of these hybrid materials for various light energy harvesting and optoelectronic applications.

INTRODUCTION

In the area of building light energy harvesting nanomaterials, all-carbon materials such as fullerene, endohedral fullerene, nanotubes, and graphene, have played a significant role.[1-7] Several key discoveries have been made to unravel the key mechanistic aspects of fundamentals of charge transfer, and in building light energy harvesting, optoelectronic and photocatalytic applications.[8-9] The basic approach in the design of such materials is in the construction of 'simple' to 'complex' donor-acceptor hybrids. The multi-modular complex systems are elegantly designed to probe competitive energy and electron transfer, sequential electron transfer and/or hole migration, and in some instances, photocatalytic electron pooling experiments. For successful energy harvesting and photocatalytic applications, the key requirement is to generate electron transfer products of appreciable lifetimes possessing high potential values (stored energy in the radical ion pairs) to drive photocatalytic reactions.[10-12]

Diameter-sorted single-wall carbon nanotubes (SWCNTs) reveal good optical coverage in the visible-near infrared (NIR) region and emit in the NIR region.[13-14] Hence, among other applications, they have been utilized in building donor-acceptor hybrids and further employing these hybrids in building light energy conversion devices.[15-25] In the 'simple' donor-acceptor construction, photosensitizers (P) are either covalently or noncovalently attached to the SWCNTs to yield P-SWCNT hybrids. Depending upon the relative energy levels of P and SWCNT, the excitation of P could promote an electron from the LUMO level to the conduction band of the SWCNT. Alternatively, an electron from the conduction band of SWCNT could transfer to the half-filled HOMO level of the photoexcited photosensitizer. The former electron transfer route would yield $P^{\bullet+}$-$SWCNT^{\bullet-}$ while the latter route would yield $P^{\bullet-}$-$SWCNT^{\bullet+}$ radical ion pairs.[2] Direct excitation of SWCNT is known to produce excitons and some instance trions.[18-20, 26] Due to relatively high binding energy and short lifetime, the exciton/trion dissociation to promote electron transfer to the LUMO level of P is rarely observed.[27] Often, the produced radical ion pairs in 'simple' P-SWCNT have been short-lived due to the proximity of donor-acceptor entities and the involvement of excitonic peaks making the spectral interpretation tedious. These issues have created a knowledge gap in understanding the role of SWCNTs in promoting and stabilizing electron transfer products.

To successfully address the above-stated issue, building multi-modular 'complex' donor-acceptor systems where the energy levels of the different donor(s) and acceptor(s) are arranged in such a way that they could promote electron migration or hole transfer from the initial cation-anion species produced by photoexcitation without losing much of energy.[28,29] However, building such systems is not only synthetically challenging but requires detailed spectroscopic, redox, and photochemical studies. In the present study, we have undertaken such an important task and report a multi-modular *molecular cleft* capable of binding diameter-sorted SWCNTs and stabilizing the charge-separated states.

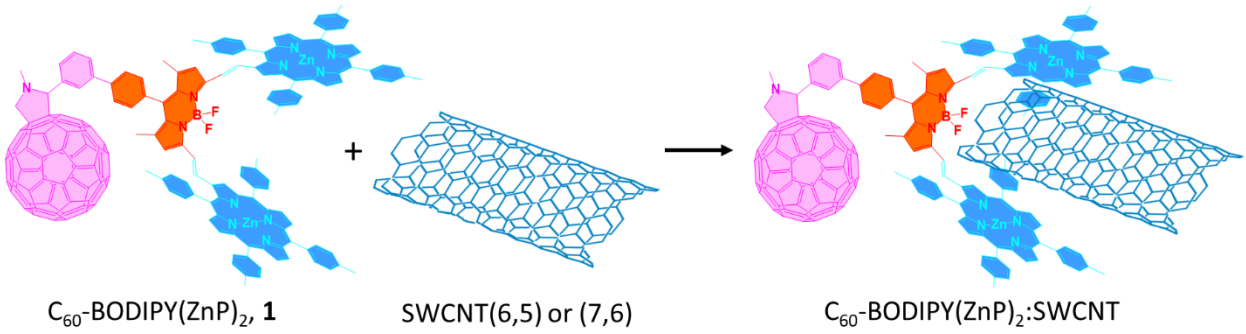

Figure 1. Structure of C_{60}-BODIP$(ZnP)_2$, **1** and its binding to diameter sorted SWCNTs to produce C_{60}-BODIP$(ZnP)_2$:SWCNT donor-acceptor nanohybrids, developed to seek photoinduced charge stabilization.

Figure 1 shows the structure of the wide band capturing *molecular cleft* **1**. The design involves a BF_2-chelated dipyrromethene (BODIPY)[30-32] carrying a charge-stabilizing electron acceptor, C_{60} positioned at the meso-position of the macrocycle. The alpha-positions of the BODIPY ring are further functionalized to carry two styryl-zinc porphyrin entities, abbreviated as C_{60}-BODIPY-(zinc porphyrin)$_2$, **1**. To maximize the π-conjugation,[33] porphyrins are functionalized at the β-pyrrole positions instead of traditionally used *meso*-phenyl positions. The consequence of this approach is to promote the optical absorption coverage to the 300-800 nm range while leaving the two zinc porphyrin (ZnP) positioned to form a molecular cleft (or tweezer) of the appropriate size to host diameter sorted SWCNTs. Commercially available size-sorted nanotubes, SWCNT(6,5) and SWCNT(7,6) have been utilized to bind **1** in the present study. In the absence of SWCNT, the excitation of BODIPY$(ZnP)_2$ in **1** would promote electron transfer involving C_{60} to produce $C_{60}^{\bullet-}$-(BODIP$(ZnP)_2)^{\bullet+}$ radical ion pair. In the **1**:SWCNT hybrids formed

upon nanotube binding, owing to the facile oxidation of SWCNTs, a hole shift is expected to produce $C_{60}^{\bullet-}$-(BODIP(ZnP)$_2$):SWCNT$^{\bullet+}$ radical ion pair. Owing to the distant location of the cation and anion radical species, charge stabilization is expected to occur in the **1**:SWCNT hybrids. Key findings on this novel system and approach are summarized in the following sections.

RESULTS AND DISCUSSION

Synthesis of C_{60}-BODIPY(ZnP)$_2$, 1

Scheme S1 in the supporting information outlines the synthesis of precursor compounds, **1a-1e**, while Scheme 1 below outlines the synthesis of the target compound, C_{60}-BODIPY-(zinc porphyrin)$_2$, **1**. Details of the synthesis along with characterization data are given in the supporting information (see Figures S1 to S15).

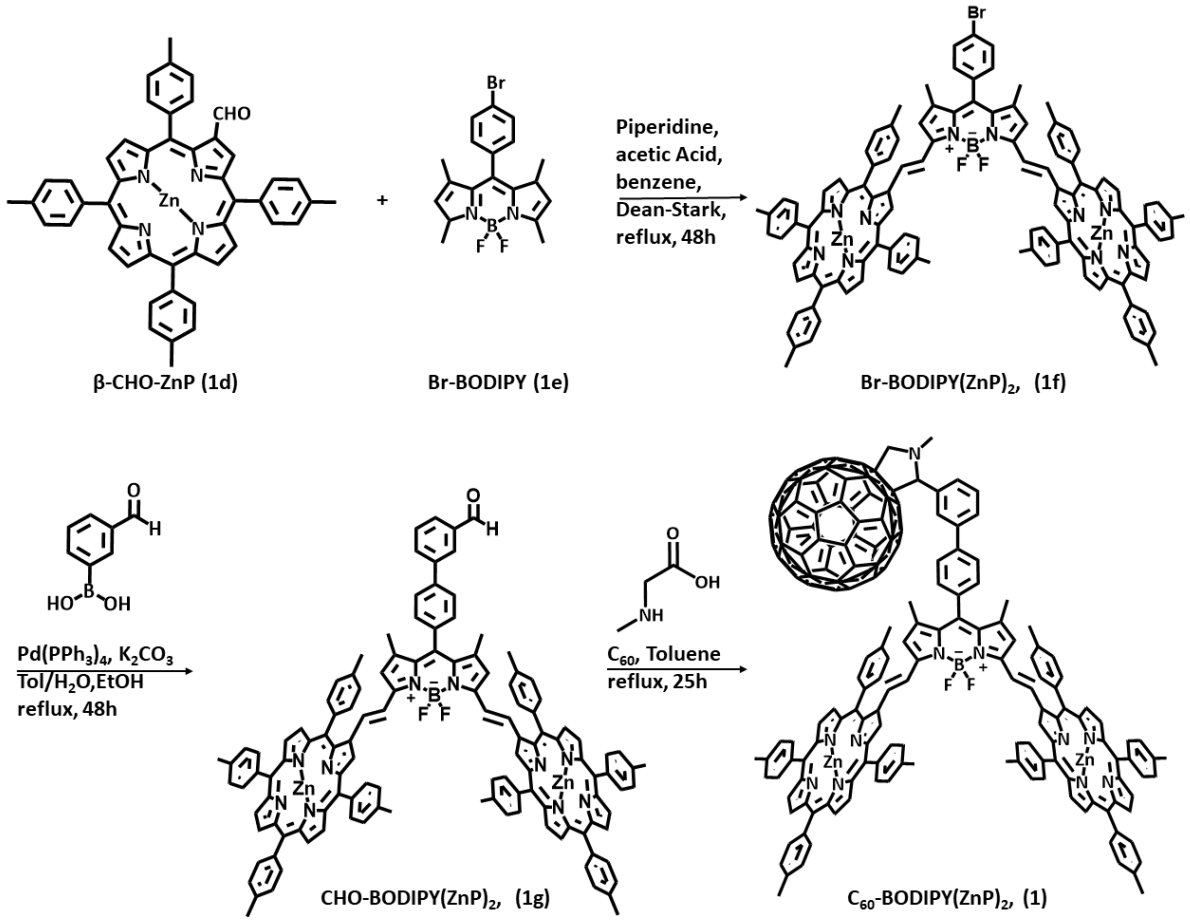

Scheme 1. Methodology used in the synthesis of C_{60}-BODIPY(ZnP)$_2$, **1.**

Briefly, free-base tetratolylporphyrin, **1a** was synthesized by condensing pyrrole and tolyl aldehyde in propionic acid followed by chromatographic separation in 21.1% yield. This was subsequently metallated using copper acetate followed by purification to get **1b** (yield = 76.33 %). 1b was subsequently formylated under Vilsmeier conditions followed by demetallation to yield β-formyl free-base porphyrin, **1c** (yield = 52.4 %). **1c** was then metallated with zinc acetate to get β-formyl zinc porphyrin, **1d** (yield = 55.0 %). In a separate experiment, 2,4-dimethylpyrrole was treated with 4-bromo benzaldehyde in tetrahydrofuran (THF) in the presence of trifluoroacetic acid (TFA) followed by treatment with dichlorodicyanobenzoquinone (DDQ) to obtain 4-bromophenylBODIPY, **1e** in 41.4% yield. Next, **1d** and **1e** were condensed in benzene containing piperidine and acetic acid using a Dean-Stark apparatus. The formation of bisstyrylBODIPY-(zinc porphyrin)$_2$, **1f** was probed spectroscopically. Upon purification, **1f** was obtained in 32.0% yield. **1f** was treated with 3-formylphenylboronic acid in the presence of K_2CO_3 and $Pd(PPh_3)_4$ catalyst to get compound **1g** in 22.9% yield. Finally, **1g** was treated with C_{60} and sarcocine in toluene followed by chromatographic separation to get the final compound **1** in 25.2% yield. The purity of the final compound was verified by thin-layer chromatography.

Absorption, emission, and electrochemical studies

Figure 2a shows the absorption spectrum of **1** and **1f**, the compound without C_{60} in dichlorobenzene (DCB). In both the compounds, the ZnP Soret band was located at 424 nm while the main Q-bands were at 560 nm and 590 nm. In addition, broad peaks that could be attributed to bisstyrylBODIPY[31] were located at 470 nm (as a shoulder with ZnP contributions) and 722 nm in the case of **1** and 734 nm in the case of **1f**. The C_{60} peak in **1** was located at 326 nm which was absent in the case of **1f.** Key points were the spectral coverage of 300-800 nm and significant spectral broadening due to extensive π-conjugation between the entities.

Interesting observations were made in fluorescence emission spectral studies. Figure 2b shows the fluorescence emission of **1** and **1f** in DCB at different excitation conditions. Compound **1f** when excited at 556 nm, predominantly exciting the ZnP entity, revealed two emission peaks at 688 and 788 nm of almost the same intensity. The first peak is red-shifted by over 85 nm compared to pristine zinc tetratolyl porphyrin due to extended π-conjugation through the β-position.[33] When **1f** was excited at 480 nm (predominantly bisstrylBODIPY with some contributions from ZnP), revealed two peaks at 688 nm and 784 nm, however, with different intensity ratios. That is, the

784 nm peak was about 4.5 times higher than that of the 688 nm peak due to contributions from the bisstyrylBODIPY entity along with that from the ZnP entity. Here, contributions of excitation transfer from ^{1}ZnP* to bisstrylBODIPY could be possible due to favorable spectral overlap.[34] In the case of **1**, when the compound was excited at 555 nm, a peak at 784 nm largely due to bisstrylBODIPY was observed. Also, when **1** was excited at 480 nm, a peak at 786 nm due to bisstrylBODIPY was observed. When **1** was excited at 720 nm, mainly exciting bisstyrylBODIPY, weak emission at 786 nm was present. The absence of ZnP peaks in **1** under ZnP excitation conditions reveals efficient excitation transfer to bisstrylBODIPY and likely not electron transfer involving C_{60} due to the large separation between them. Interestingly, the quenched intensity of bisstrylBODIPY in **1** compared to that in **1f** under both excitation conditions (40-60% quenching) suggests that the ^{1}bisstyrylBODIPY* in **1** (formed either by direct excitation or through the mechanism of energy transfer) undergoes further photochemical events involving C_{60}.[34]

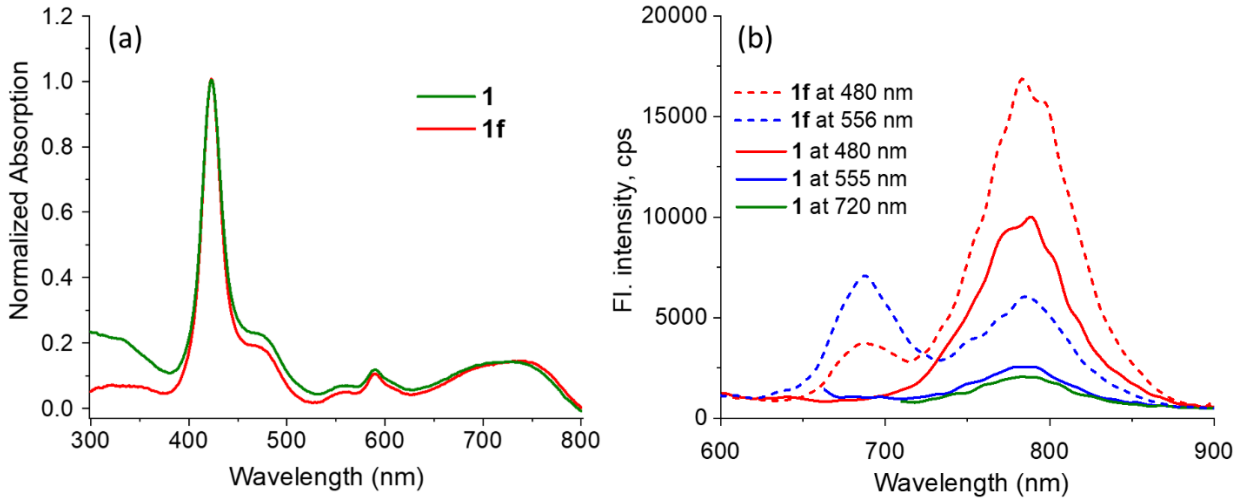

Figure 2. (a) Normalized absorption and (b) fluorescence of **1** and **1f** in DCB under different excitation conditions.

The redox potentials of the investigated compounds were measured in DCB containing 0.1 M (TBA)ClO_4 using differential pulse voltammetry (DPV) as they help in establishing energetics associated with various photochemical events. As shown in Figure 3a, **1f** revealed the first oxidation at 0.86 V vs. Ag/AgCl and the three reductions at -0.64 V, -0.89, and -1.34 V. The first oxidation had about twice the currents than that of the reduction. By comparison with earlier reported β-pyrrole functionalized porphyrin[33] and bisstyrylBODIPY,[29] the first oxidation is

ascribed to involve both ZnP and BODIPY entities while the first reduction to BODIPY and the subsequent reductions to the ZnP entities. Compound **1** with an additional C_{60} entity, revealed additional reductions. The first reduction corresponding to C_{60} was located at -0.57, while the second broad-intense signal had contributions from the second reduction of C_{60}, the first reduction of BODIPY and ZnP. The electrochemical redox gap, $\Delta E_{1/2}$, measured as the gap between the first oxidation and first reduction, for **1f** was 1.50 V while that for **1** it was 1.39 V. That is, the presence of C_{60} in **1** lowered the overall $\Delta E_{1/2}$ gap.

Tanaka et. al. reported on the redox potentials of a series of SWCNTs of different chirality using the photoluminescence potentiometric method.[35] This technique instead of normally used DPV or cyclic voltammetry was needed due to the negligible solubility of SWCNTs, especially in the presence of 0.1M supporting electrolyte. The reported oxidation potential for SWCNT(6,5) was 0.64 V and for SWCNT(7,6) it was 0.50 V vs. Ag/AgCl. These potentials are sufficiently lower than that observed for the first oxidation of **1** (0.86 V vs. Ag/AgCl) establishing the role of the nanotubes as the final electron donors (hole shifting agent) upon binding to **1** (*vide supra*)

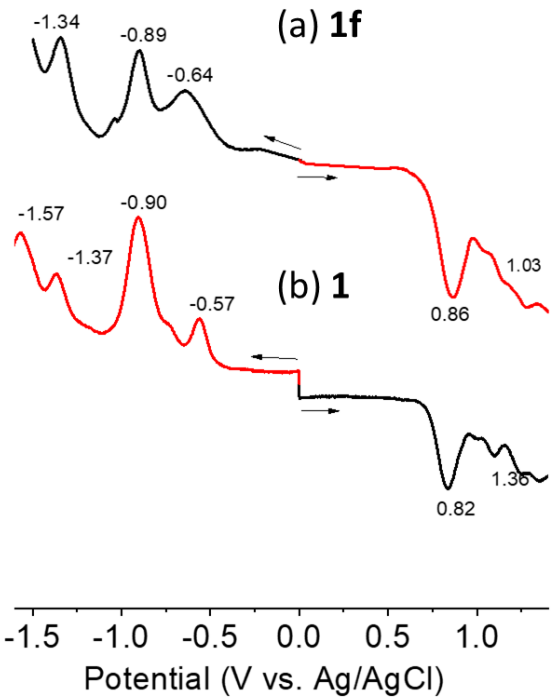

Figure 3. Differential pulse voltammograms of (a) **1f** and (b) **1** in DCB containing 0.1M $(TBA)ClO_4$.

The computational studies using Cam-B3LYP/6-31G(d,p) basis set and functional[37,38] performed on **1** also helped in visualizing their geometry and electronic structure to support the redox properties. Figure 4 shows the structure of the optimized geometry and the frontier HOMO-1, HOMO, and LUMO of **1**. The *molecular cleft* feature of the bisstyrtlBODIPY carrying two zinc porphyrin units is clear from the optimized structure. The Zn-Zn distance between the two ZnP entities was found to be 11.2Å and the distance between the meso-carbons that are located at the far end of BODIPY was found to be 12.4Å. This suggests that **1** could easily accommodate both SWCNT(6,5) (diameter = 7.6Å) and SWCNT(7,6) (diameter = 9.1Å). Additionally, the center-to-center distance between C_{60} to BODIPY (at the boron site) was 12.7Å while the distance between the center of C_{60} to Zn of ZnP entities was 17.4Å and 21.9Å, respectively. The boron to zinc distances were 8.2Å and 9.3Å. The structure also suggests a lack of steric crowding among the four redox/photoactive entities.

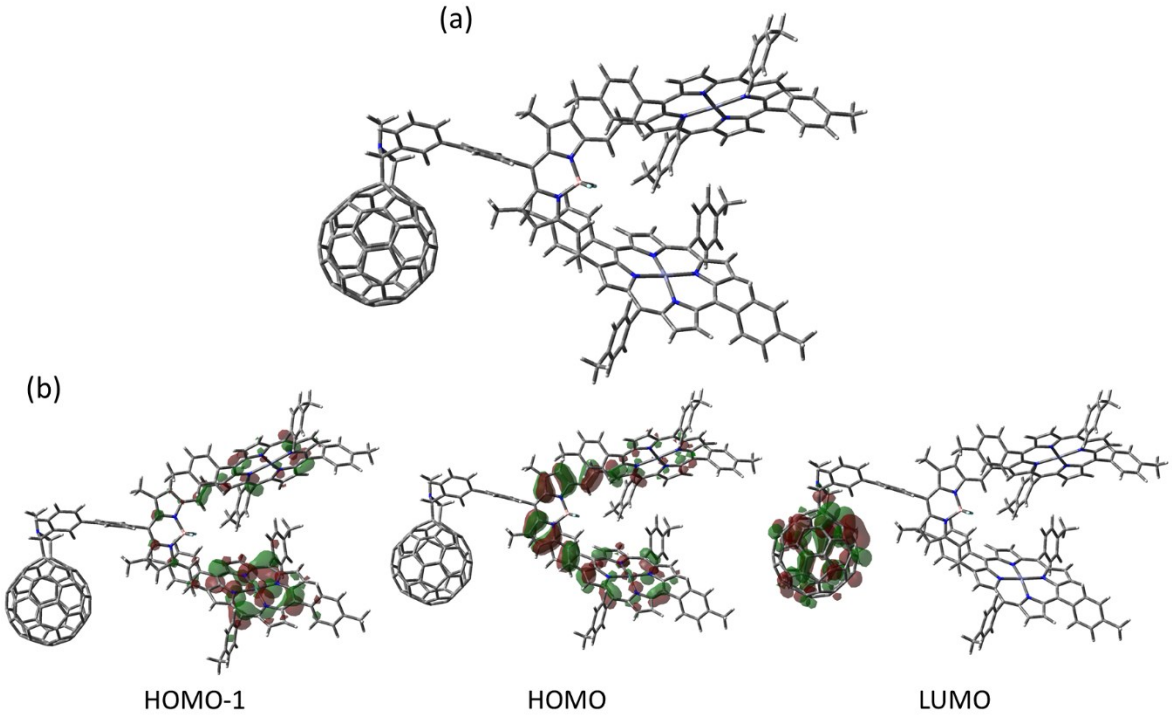

Figure 4. (a) Cam-B3LYP/6-31G(d,p) optimized geometry and (b) frontier orbitals of **1**.

A large portion of the frontier HOMO at -4.72 eV was found to be on BODIPY with significant contributions to the ZnP entities. Similarly, the HOMO-1 at -4.92 eV was mainly on the ZnP entities with a small contribution of the BODIPY. As expected, the LUMO at -3.81 eV

was fully localized on the C_{60}. The gas phase calculated HOMO-LUMO gap was found to be 0.91 eV slightly lower than that calculated from electrochemical measurements. The energetically close HOMO and HOMO-1 and their distributions are consistent with the oxidation of **1** with overlapped bisstryrylBODIPY and ZnP peaks.

SWCNTs binding to 1

The *molecular cleft* design of **1** is expected to bind SWCNTs via π-stacking of ZnP entities. UV-visible and fluorescence titrations were initially performed to witness SWCNTs binding to **1** in DCB. Figures 5a and b show the absorption and fluorescence spectral changes observed during (6,5) and (7,6) nanotubes binding to **1** in DCB. For this, the nanotubes were dispersed in DCB by probe sonication and the suspended particles were filtered out. In both cases, the ZnP Soret band

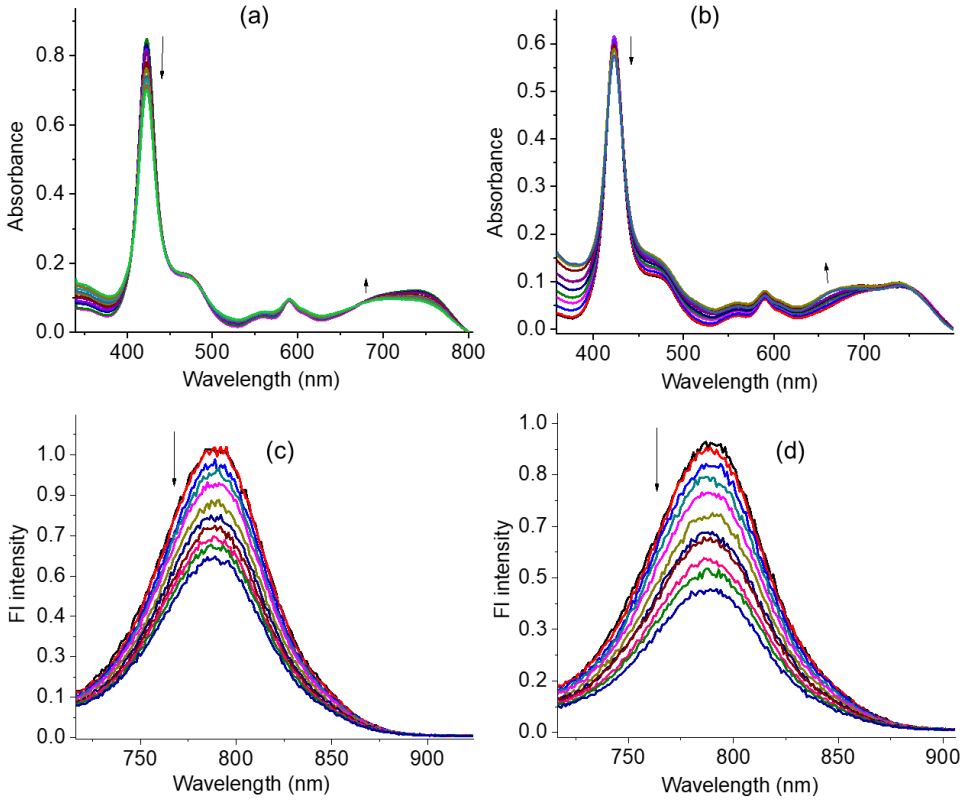

Figure 5. Absorption (a and b) and fluorescence (c and d) spectral changes observed for **1** during the binding of SWCNT(6,5) (a and c) and SWCNT(7,6) (b and d) in DCB. The samples were excited corresponding to the Soret band position.

witnessed a decrease in intensity while the far-red bisstyrylBODIPY peak revealed a blue shift. These changes were accompanied by four isosbestic points. Additional fluorescence quenching of **1** was also witnessed during SWCNT binding as shown in Figures 5c and d. About 50-60% quenching of the original intensity was observed. The combined results shown in Figure 5 indicate the role of nanotubes in further modulating the photochemical events in **1**:SWCNT hybrids.

Laser Raman spectral studies performed on the hybrids formed by pristine SWCNT(6,5) and SWCNT(7,6) and its hybrid with **1f** indeed provided additional evidence of **1f**-SWCNT hybrid formation, as shown in Figure S16. The D, G, and G' bands of pristine SWCNTs[38] revealed a shift of 2-6 cm^{-1} upon binding to **1f**. These results suggest the interaction of **1f** with SWCNTs. The relatively small shift of 2-6 cm^{-1} shift compared to ~9 cm^{-1} reported earlier for covalently functionalized SWCNT[39] is consistent with the non-covalent functionalization via π-stacking methodology using *molecular cleft* developed in the present study.

^{1}H NMR spectral studies on SWCNT binding to **1f** in $CDCl_3$ were also performed, as shown in Figures S17 and S18 in SI for (6,5) and (7,6) nanotube binding, respectively. A downward shift accompanied by spectral broadening of the peaks corresponding to the zinc porphyrin segment was observed further supporting the binding of **1f** to the nanotubes. Slow settling of the **1f**:SWCNT hybrids with time was also noted. Due to these experimental complexities, our attempts to measure the binding constant resulted in values of high uncertainty. Hence, the binding constant values are not reported here.

The Cam-B3LYP/6-31G(d,p) optimized structures of **1**:SWCNT(6,5) and **1**:SWCNT(7,6) and the frontier HOMO and LUMO for **1:**SWCNT(6,5) is shown in Figure 6. The molecular cleft hosting both diameter sorted nanotubes without steric hindrance is borne out from this exercise. The closest distance between the C_{60} carbon atom to the SWCNT carbon atom was 3.6Å for **1**:SWCNT(6,5) and 3.8Å for **1**:SWCNT(7,6) suggesting distal separation of these entities in the nanohybrid. Importantly, the HOMO was found to be on the SWCNTs in both hybrids (see Figure S19 for the HOMO and LUMO of **1**:SWCNT(7,6)) and the LUMO was localized on the C_{60} entity, a requirement to observe sequential electron transfer leading to charge stabilization.

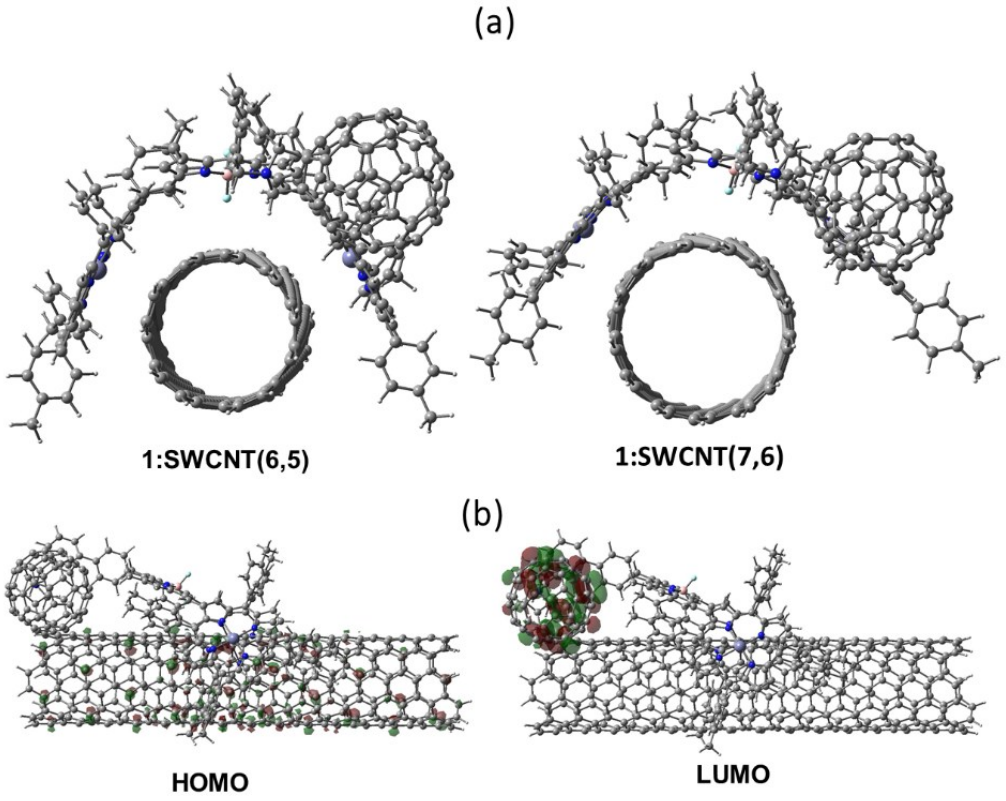

Figure 6. (a) Cam-B3LYP/6-31G(d,p) optimized structures of **1**:SWCNT(6,5) and **1**:SWCNT(7,6), and (b) frontier HOMO and LUMO for **1:**SWCNT(6,5).

Energy profile diagram

Scheme 2 below shows the different anticipated photochemical events along with their energetics. The driving forces for charge separation ($-\Delta G_{CS1}$ and $-\Delta G_{CS2}$), hole shift ($-\Delta G_{HS}$), and electron migration ($-\Delta G_{EM}$) are calculated according to equations (1-4). The solvation term was neglected in these calculations due to large donor-acceptor separations.

$$-\Delta G_{CS1} = \Delta E_{0,0} - (E_{ox}^{1} - E_{red}^{1}) \quad (1)$$

$$-\Delta G_{CS2} = \Delta E_{0,0} - (E_{ox}^{2} - E_{red}^{2}) \quad (2)$$

$$-\Delta G_{HS} = \Delta G_{CS1} - (E_{ox}^{2} - E_{ox}^{1}) \quad (3)$$

$$-\Delta G_{EM} = \Delta G_{CS2} - (E_{red}^{2} - E_{red}^{1}) \quad (4)$$

where E_{ox}^1 is the oxidation potential for the BODIPY$^{0/\bullet+}$ process (0.82 V), E_{ox}^2 is the oxidation potential for the SWCNT$^{0/\bullet+}$ process (0.64 V for (6,5) and 0.50 V for (7,6)), E_{red}^1 is the reduction potential for the $C_{60}^{0/\bullet-}$ process (-0.57 V) and E_{red}^2 is the reduction potential for the BODIPY$^{0/\bullet-}$ process (-0.64 V) in the **1**-SWCNT hybrids. $\Delta E_{0,0}$ is the energy of the 0-0 transition of the lowest excited state of the BODIPY (1.65 eV) and ZnP (1.95 eV), evaluated as the average energies of absorption and fluorescence peaks corresponding to the 0,0 transitions. Owing to the efficient energy transfer from ^{1}ZnP* to produce ^{1}bisstyrylBODIPY*, all electron transfer events are assumed to be initiated from ^{1}bisstyrylBODIPY* (either directly excited or formed as an energy transfer product), and its energy is used in the calculations.

Such an energy profile scheme, although relatively complex, demonstrates the thermodynamic feasibility of different processes, similar to the processes taking place in natural photosynthesis.[41] Exciting **1** at one of the BODIPY peaks would generate ^{1}BODIPY*. This species could also be generated by exciting ZnP through thermodynamically feasible EET. As mentioned earlier, due to good spectral overlap such a process is expected to be very efficient. The ^{1}BOIDPY* in **1** could undergo reductive electron transfer following two paths, viz., CS1 involving C_{60} electron acceptor to generate $C_{60}^{\bullet-}$-[BODIPY(ZnP)$_2$]$^{\bullet+}$-SWCNT. Due to almost the same oxidation potentials and delocalization of the HOMO on both BODIPY and ZnP entities, we have considered the formation of [BODIPY(ZnP)$_2$]$^{\bullet+}$ instead of the radical cation residing solely on the BODIPY or ZnP entities. In CS2, the ^{1}BODIPY* could undergo oxidative electron transfer involving SWCNT to produce C_{60}-[BODIPY(ZnP)$_2$]$^{\bullet-}$-SWCNT$^{\bullet+}$. The facile oxidation of SWCNT makes this thermodynamically feasible (see the -ΔG values listed for each process in Scheme 2).

In the subsequent dark reactions, the product of CS1, $C_{60}^{\bullet-}$-[BODIPY(ZnP)$_2$]$^{\bullet+}$-SWCNT could undergo a hole shift reaction with SWCNT to produce $C_{60}^{\bullet-}$-BODIPY(ZnP)$_2$-SWCNT$^{\bullet+}$. Similarly, the product of CS2, C_{60}-[BODIPY(ZnP)$_2$]$^{\bullet-}$-SWCNT$^{\bullet+}$, could undergo an electron migration reaction involving easily reducible C_{60} to produce $C_{60}^{\bullet-}$-BODIPY(ZnP)$_2$-SWCNT$^{\bullet+}$. It is important to note that irrespective of the path it follows, the final electron transfer product would be the same, i.e., $C_{60}^{\bullet-}$-BODIPY(ZnP)$_2$-SWCNT$^{\bullet+}$, before returning to the ground state (charge recombination, CR in Scheme 2). Due to the distant positioning of the radical cation and radical anion, charge stabilization is expected to occur should the **1**:SWCNT nanohybrid follow the electron transfer path described here.

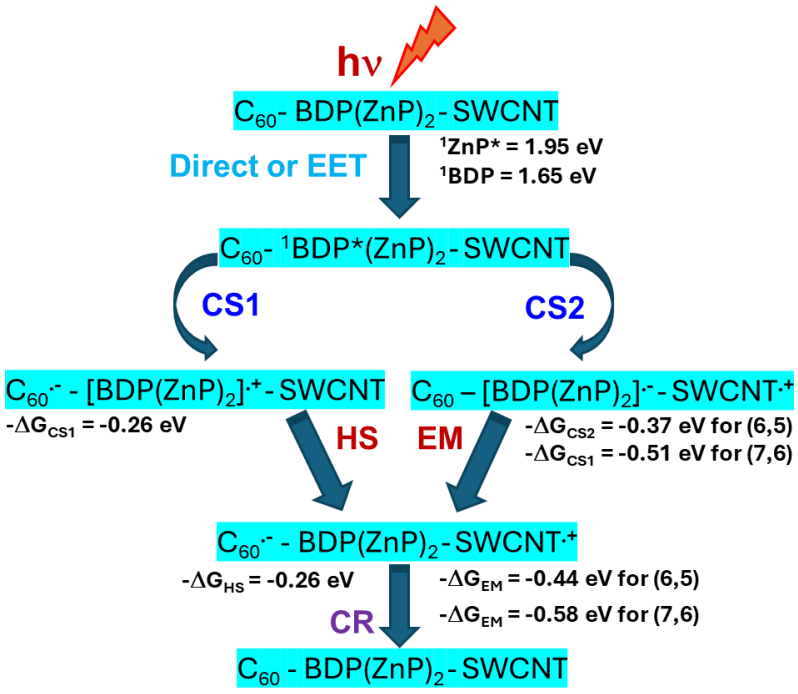

Scheme 2. Different photochemical and subsequent dark energy and electron transfer events along with their energetics of **1**:SWCNT multi-modular donor-acceptor hybrids. See text for details for energetics calculations. CS=charge separation, HS=hole shift, EM=electron migration, CR=charge recombination, EET=excitation energy transfer, BDP=bisstrylBODIPY, ZnP=zinc porphyrin, and C_{60}-BDP(ZnP)$_2$ = **1**. All the photochemical events are assumed to be initiated from ^{1}BDP* formed either by direct excitation or formed as an energy transfer product of ^{1}ZnP*.

Femtosecond transient absorption studies.

The above-summarized results nicely showcase the possible light-induced and dark electron transfer events resulting in charge-stabilized states in which the noncovalently bound nanotubes would take an active role. To demonstrate such a process femtosecond transient absorption studies were systematically performed, and the results are summarized below.

Figure 7a shows the femtosecond transient absorption spectra (fs-TA) of **1f** at the excitation wavelength of 650 nm corresponding to the bisstyrylBODIPY entity at the indicated delay times. The spectrum recorded at 1 ps delay time revealed excited state absorption (ESA) peaks at 532, 625, 780, 1064, and 1310 nm. Based on earlier reported studies, the 1310 nm peak could be attributed to singlet-singlet absorption.[43] In addition to this, peaks negative peaks at 470, 702, and 740 nm were observed. By comparison with the earlier discussed absorption and fluorescence

spectrum, the first two negative peaks were possible to assign to the ground state bleaching (GSB) and the 740 nm peak to the stimulated emission (SE) of the bisstyrylBODIPY entity of **1f**. The fs-TA spectrum was also recorded by exciting the sample corresponding to ZnP Soret and visible peak maxima. In both cases, the first recordable spectrum at 1 ps was identical to that obtained when bisstyrylBODIPY was directly excited. This indicates the occurrence of ultrafast energy transfer from ^{1}ZnP* to bisstyrylBODIPY to produce ^{1}bisstyrylBODIPY* ($k_{EET} > 1.0 \times 10^{12}$ s^{-1}) in **1f**. Within the next 3 ns, the decay and recovery of the positive and negative peaks were observed, however, still retaining some of the original intensity and without any noticeable new peaks. This suggests the ^{1}bisstyrylBODIPY* undergoes intersystem crossing ($E_T \sim 1.26$ eV) slowly to populate the ^{3}bisstyrylBODIPY*.

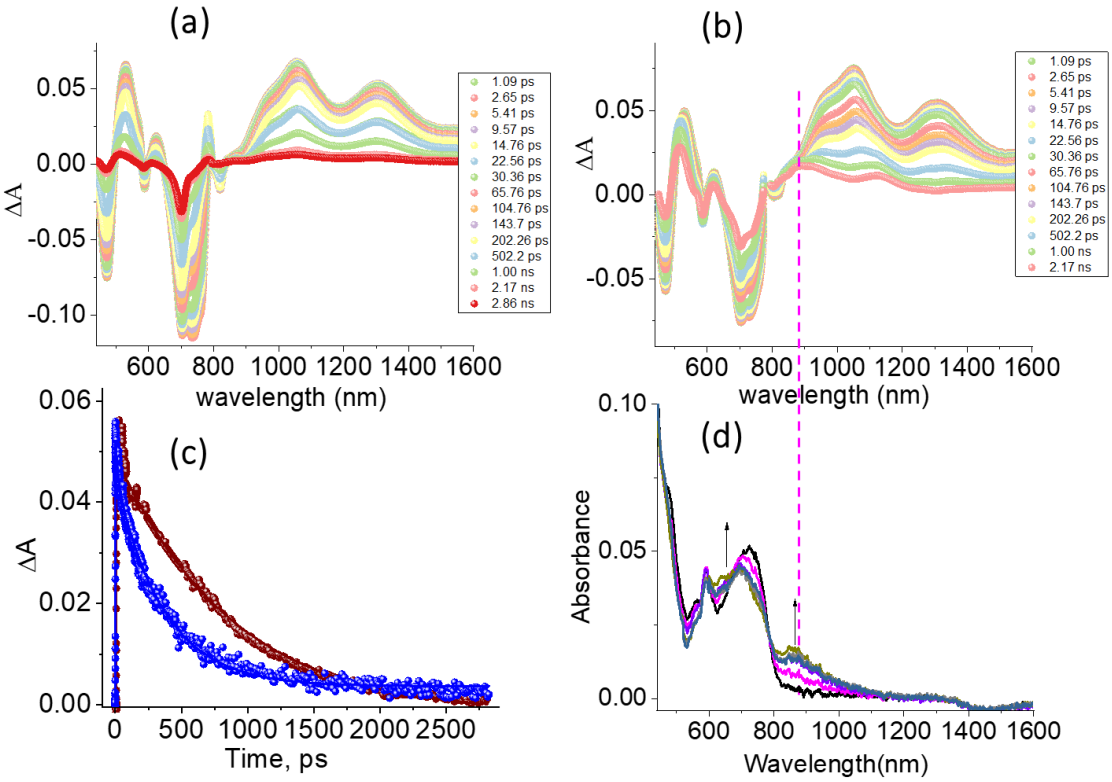

Figure 7. Fs-TA spectra at the indicated delay time of (a) **1f** and (b) **1** in DCB at the excitation wavelength of 650 nm. (c) Decay profile of the 1306 nm peak of **1f** (brown) and **1** (blue). (d) spectroelectrochemical oxidation of **1** revealing the spectrum of **1**$^{\bullet+}$.

The presence of C_{60} in **1** revealed significant transient spectral changes supporting the occurrence of charge separation as shown in Figure 7b. Here, the initial spectrum recorded at 1 ps had features similar to **1f** concerning the ESA, GSB, and SE peaks. Decay/recovery of the positive

and negative signals results in new peaks ~ 900 nm expected for the $[BODIPY(ZnP)_2]^{\bullet+}$ along with a shoulder peak ~ 1000 nm expected for $C_{60}^{\bullet-}$. The $[BODIPY(ZnP)_2]^{\bullet+}$ peak was confirmed by performing spectroelectrochemical studies by applying a potential corresponding to the first oxidation of **1** in a thin-layer spectroelectrochemical cell as shown in Figure 7d. Other peaks corresponding to $[BODIPY(ZnP)_2]^{\bullet+}$ were also present confirming the formation of $[BODIPY(ZnP)_2]^{\bullet+}$-$C_{60}^{\bullet-}$charge-separated state in **1.**

To evaluate the rate constant for charge separation, k_{CS}, the kinetics of the ESA peak at 1310 nm for both **1f** and **1** was monitored as shown in Figure 7c. Faster decay of **1** compared to **1f** was evident. From these decay constants, and assuming the rapid decay in **1** was due to electron transfer, the rate constant for charge separation, k_{CS} was evaluated and found to be 1.77×10^9 s^{-1} indicating fairly efficient electron transfer considering relatively a large distance between them.

Next, fs-TA spectral studies on **1**:SWCNT(6,5) and **1**:SWCNT(7,6) in DCB were performed by complexing the nanotubes, as shown in Figure 8. At the excitation wavelength of 650 nm, the spectrum recorded at 1 ps was close to that observed for **1** in the absence of bound nanotubes indicating the formation of the ^{1}bisstyrylBODIPY* in the hybrids (Figure 8a and 8c). The decay and recovery of the positive and negative peaks revealed peaks expected for the $[BODIPY(ZnP)_2]^{\bullet+}$ species in the 900 nm region, however, they were relatively short-lived. Contributions from the signature peak of $C_{60}^{\bullet-}$ in the 1000 nm, although relatively weak, were present. This suggests the $[BODIPY(ZnP)_2]^{\bullet+}$ is likely undergoing a hole shift involving the bound SWCNT. The k_{CS} was calculated by monitoring the time profile of the ESA peak at 1310 nm and was found to be 7.46×10^9 s^{-1} for **1**:SWCNT(6,5) and 4.18×10^9 s^{-1} 1:SWCNT(7,6) (see Figures 8b and d for decay plots). The presence of SWCNT promoted electron transfer involving both CS1 and CS2 mechanisms. Assuming the magnitude of CS1 remains the same as that in pristine **1**, values of k_{CS} for CS2 were calculated and found to be 5.69×10^9 s^{-1} for **1**:SWCNT(6,5) and 2.41×10^9 s^{-1} **1**:SWCNT(7,6). Higher magnitudes of CS2 are understandable based on the higher exothermicity of these reactions (see Scheme 2).

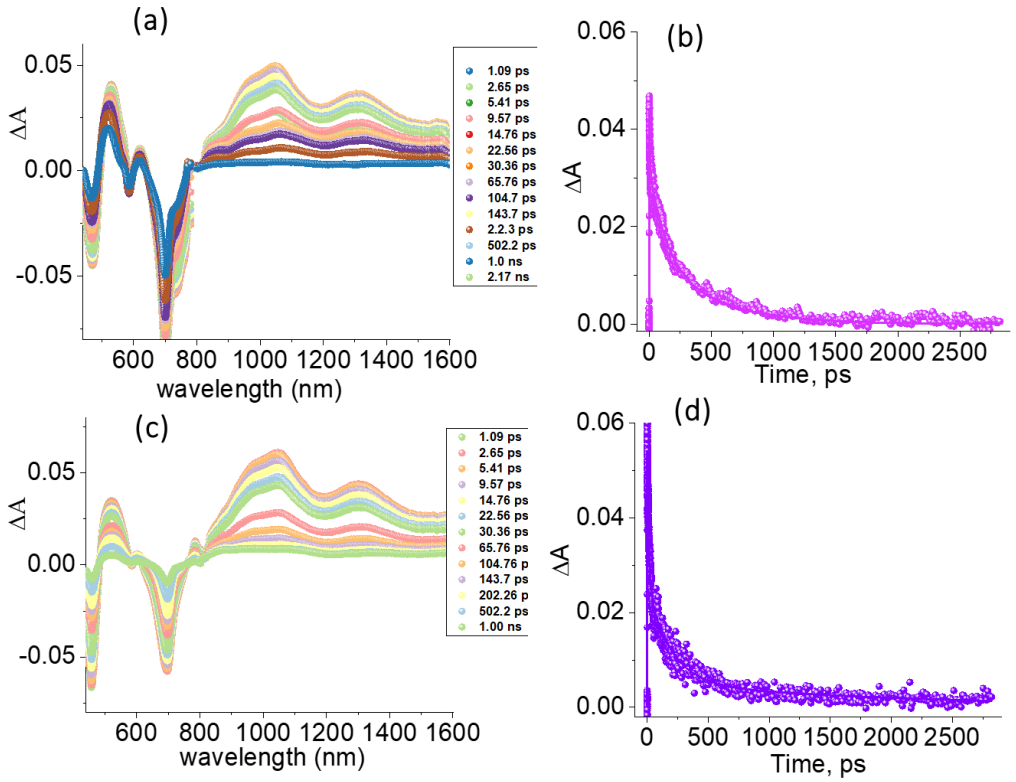

Figure 8. (a and c) Fs-TA spectra at the indicated delay times of **1**:SWCNT(6,5) and **1**:SWCNT(7,6) in DCB at the excitation wavelength of 650 nm. The respective decay profiles of the ESA peak at 1310 are shown in Figures 8b and d.

To evaluate the persistence of the charge-separated states, the fs-TA data was subjected to GloTarAn-Target analysis,[44-45] and results from such data analysis are shown in Figure 9. The data was subjected to an S_1 → CS → GS model (GS = ground state). The species-associated spectra (SAS) and population time profiles are shown in Figure 9a. The SAS for the CS state largely agreed with the peaks expected for the charge-separated state. From this, the lifetime for S_1 and CS were calculated to be 111 ps and 1.66 ns. Here, the lifetime refers to the average lifetime of a given state. For **1**:SWCNT(6,5) and **1**:SWCNT(7,6), a two-step model representing CS1/CS2 (light-induced) and HS/EM (subsequent dark reaction) was satisfactory, as shown in the plots of Figures 9b and c. Such analysis yielded lifetimes of 6.4 ps and 3.33 ns representing CS1 and HS in the case of **1**:SWCNT(6,5), and 15.5 ps and 3.54 ns representing CS2 and EM for **1**:SWCNT(7,6). The final lifetime is the overall lifetime of the $C_{60}^{\bullet-}$-BODIPY(ZnP)$_2$-SWCNT$^{\bullet+}$ state with distinctly positioned anion and cation radical species. That is, the average CS lifetime of 1.66 ns obtained for **1** in the absence of nanotubes was improved to 3.33 ns and 3.54 ns, almost

double, upon binding to nanotubes of (6,5) and (7,6) chirality. Due to the facile oxidation of SWCNT(7,6) compared to SWCNT(6,5), a comparatively better charge stabilization is witnessed in the case of **1**:SWCNT(7,6) (3.54 ns), compared to **1**:SWCNT(6,5) (3.33 ns). Although these values are of the same magnitude (3.33 ns vs. 3.54 ns), the subtle changes in charge stabilization between the two nanotubes are noticeable.

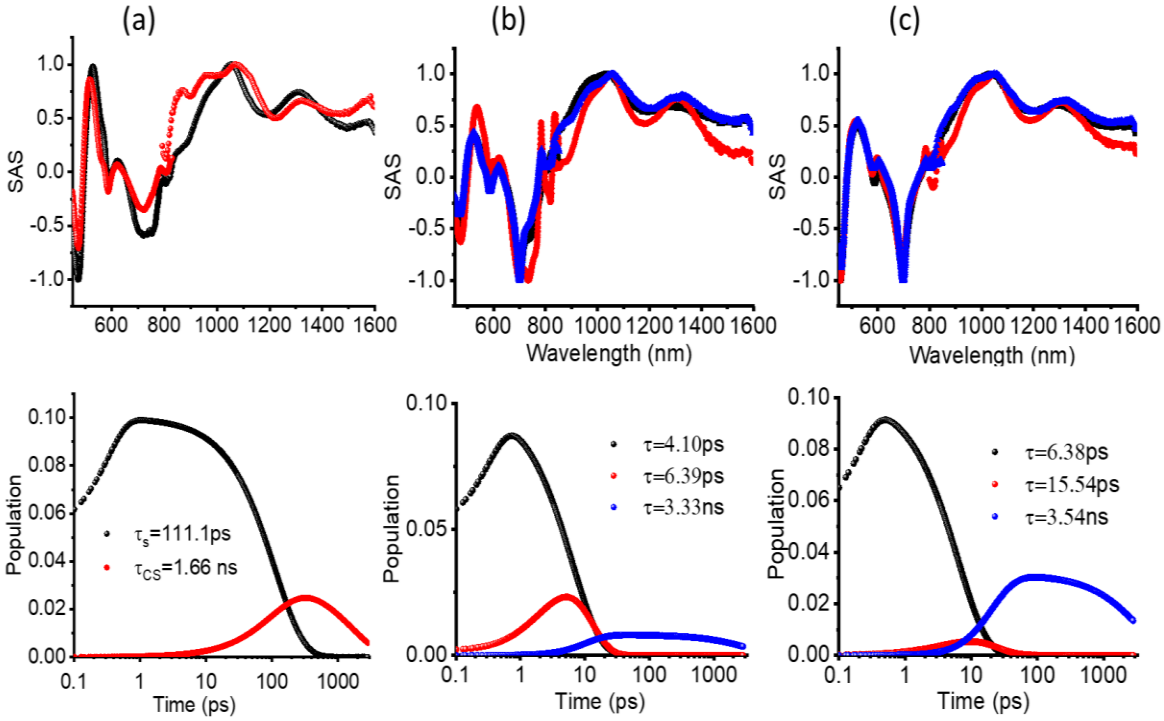

Figure 9. Results of GloTarAn-Target analysis of the fs-TA data for (a) **1**, (b) **1**:SWCNT(6,5), and (c) **1**:SWCNT(7,6). The respective population time profiles are given below each plot.

CONCLUSIONS

In conclusion, the significance of diameter-sorted single-wall carbon nanotubes (SWCNTs) in prolonging the lifetime of the charge-separated states in the multi-modular donor-acceptor *molecular cleft* is successfully demonstrated. The newly synthesized for this purpose, a wide-band capturing, C_{60}-bisstyrylBODIPY-(zinc porphyrin)$_2$, *molecular cleft* **1**, was successfully shown, using several physicochemical and computations methods, to bind both SWCNT(6,5) and SWCNT(7,6) and to form stable nanohybrids. The constructed energy profile diagram revealed that both the nanotubes upon binding to **1** act as hole-shifting agents during the photo-induced

electron transfer resulting in distant separation of radical ion-pair species promoting charge stabilization. Fs-TA studies followed by data analysis by GloTarAn-Target analysis provided conclusive evidence for such reaction pathways. While the lifetime of charge separated state persisted for about 1.66 ns in the case of donor-acceptor, **1**, binding to SWCNTs prolonged the lifetime twice as much. The present study brings out the significance of molecularly engineered nanohybrids featuring a wideband capturing donor-acceptor chromophore binding to low bandgap SWCNTs in stabilizing the much-desired charge-separated states.

ASSOCIATED CONTENT

Supporting Information

The supporting information is available free of charge at https://pubs.acs.org/doi...

Experimental section, synthetic details along with characterization data, Raman spectra of the hybrids, and additional computational spectral data.

Conflict of interest

The authors declare no conflict of interest.

AUTHOR INFORMATION

Corresponding Author

Francis D'Souza - Department of Chemistry, University of North Texas, 1155 Union Circle, #305070, Denton, TX 76203-5017, United States. ORCID: https://orcid.org/0000-0003-3815-8949, E-mail: Francis.Dsouza@unt.edu

Authors

Shahrzad Kazemi - Department of Chemistry, University of North Texas, 1155 Union Circle, #305070, Denton, TX 76203-5017, United States

Ajyal Z. Alsale - Department of Chemistry, University of North Texas, 1155 Union Circle, #305070, Denton, TX 76203-5017, United States

Current address: Chemistry Department, Imam Abdulrahman bin Faisal University, Dammam, 34212, Saudi Arabia.

Paul A. Karr - Department of Physical Sciences and Mathematics Wayne State College, 1111 Main Street, Wayne, Nebraska, 68787, United States

ACKNOWLEDGMENTS

This research was supported by the US-National Science Foundation (2000988 and 2345836 to FD). The computational work was performed at the Holland Computing Center of the University of Nebraska, which receives support from the Nebraska Research Initiative.

REFERENCES

1. Bottari, G.; Herranz, M. A.; Wibmer, L.; Volland, M.; Rodriguez-Perez, L.; Guldi, D. M.; Hirsch, A.; Martin, N.; D'Souza, F.; Torres, T. Chemical functionalization and characterization of graphene-based materials. *Chem. Soc. Rev.* **2017***, 46*, 4464.

2. Barrejon, M.; Arellano, L. M.; D'Souza, F.; Langa, F. Bidirectional charge-transfer behavior in carbon-based hybrid. *Nanoscale* **2019**, *11,* 14978.

3. Blackburn, J. L. Semiconducting single-walled carbon nanotubes in solar energy harvesting. *ACS Energy Lett.* **2017***, 2*, 1598.

4. Du, L.; Xiong, W.; Chan, W. K.; Phillips, D. L. Photoinduced electron transfer processes of single-wall carbon nanotube (SWCNT)–based hybrids. *Nanophotonics* **2020***, 9*, 4689.

5. Bottari, G.; De La Torre, G.; Guldi, D. M.; Torres, T. Covalent and noncovalent phthalocyanine−carbon nanostructure systems: synthesis, photoinduced electron transfer, and application to molecular photovoltaics. *Chem. Rev.* **2010***, 110*, 6768.

6. Strauss, V.; Roth, A.; Sekita, M.; Guldi, D. M. Efficient energy-conversion materials for the future: understanding and tailoring charge-transfer processes in carbon nanostructures. *Chem.* **2016***, 1*, 531.

7. D'Souza, F.; Ito, O. Photosensitized electron transfer processes of nanocarbons applicable to solar cells. *Chem. Soc. Rev.* **2012***, 41*, 86.

8. Kim S. H. *et al.* Harvesting electrical energy from carbon nanotube yarn twist. *Science* **2017**, *357*, 773.

9. Wang, L.; Liu, H.; Konik, R. M.; Misewich, J. A.; Wong, S. S. Carbon nanotube-based heterostructures for solar energy applications. *Chem. Soc. Rev.* **2013***, 42*, 8134.

10. D'Souza, F.; Sandanayaka, A. S. D.; Ito, O. SWNT-based supramolecular nanoarchitectures with photosensitizing donor and acceptor molecules. *J. Phys. Chem. Lett.* **2010***, 1*, 2586.

11. Ohkubo, K.; Fukuzumi, S. Long-lived charge-separated states of simple electron donor-acceptor dyads using porphyrins and phthalocyanines. *J. Porphyrins Phthalocyanines* **2008**, *12*, 993.

12. Umeyama, T.; Imahori, H. Electron transfer and exciplex chemistry of functionalized nanocarbons: effects of electronic coupling and donor dimerization. *Nanoscale Horiz.* **2018***, 3*, 352.

13. Tsyboulski, D. A.; Bachilo, S. M.; Weisman, R. B. Versatile visualization of individual single-walled carbon nanotubes with near-infrared fluorescence microscopy. *Nano Lett.* **2005***, 5*, 975.

14. Shastry, T. A.; Hersam, M. C. Carbon nanotubes in thin-film solar cells. *Adv. Energy Mater*. **2017**, *7*, 1601205.

15. Schuettfort, T.; Nish, A.; Nicholas, R. J. Observation of a type II heterojunction in a highly ordered polymer−carbon nanotube nanohybrid structure. *Nano Lett.* **2009***, 9*, 3871.

16. Bellisario, D. O.; Jain, R. M.; Ulissi, Z.; Strano, M. S. Deterministic modelling of carbon nanotube near-infrared solar cells. *Energy Environ. Sci.* **2014***, 7*, 3769.

17. Dresselhaus, M. S.; Dresselhaus, G.; Saito, R.; Jorio, A. Exciton photophysics of carbon nanotubes. *Annu. Rev. Phys. Chem.* **2007***, 58*, 719.

18. Olivier, J.-H.; Park, J.; Deria, P.; Rawson, J.; Bai, Y.; Kumbhar, A. S.; Therien, M. J. Unambiguous diagnosis of photoinduced charge carrier signatures in a stoichiometrically controlled semiconducting polymer-wrapped carbon nanotube assembly. *Angew. Chem. Int. Ed.* **2015**, *54*, 8133.

19. Tagmatarchis, N.; Prato, M.; Guldi, D. M. Soluble carbon nanotube ensembles for light-induced electron transfer interactions. *Physica E: Low-dimensional Systems and Nanostructures* **2005***, 29*, 546.

20. Ballesteros, B.; De La Torre, G.; Ehli, C.; Aminur Rahman, G. M.; Agullo-Rueda, F.; Guldi, D. M.; Torres, T. Single-wall carbon nanotubes bearing covalently linked phthalocyanines − photoinduced electron transfer. *J. Am. Chem. Soc.* **2007***, 129*, 5061.

21. Romero-Nieto, C.; Garcia, R.; Herranz, M. A; Ehli, C.; Ruppert, M.; Hirsch, A.; Guldi, D. M.; Martin, N. Tetrathiafulvalene-based nanotweezers—noncovalent binding of carbon nanotubes in aqueous media with charge transfer implications. *J. Am. Chem. Soc.* **2012***, 134*, 9183.

22. Saito, K.; Ohtani, M.; Fukuzumi, S. Electron-transfer reduction of cup-stacked carbon nanotubes affording cup-shaped carbons with controlled diameter and size. *J. Am. Chem. Soc.* **2006***, 128*, 14216.

23. Menon, A.; Münich, P. W.; Wagner, P.; Officer, D. L.; Guldi, D. M. Amphiphilic zinc porphyrin single-walled carbon nanotube hybrids: efficient formation and excited state charge transfer studies. *Small* **2021***, 17*, 2005648.

24. Baskaran, D.; Mays, J. W.; Zhang, X. P.; Bratcher, M. S. Carbon nanotubes with covalently linked porphyrin antennae: photoinduced electron transfer. *J. Am. Chem. Soc.* **2005***, 127*, 6916.

25. D'souza, F.; Das, S. K.; Zandler, M. E.; Sandanayaka, A. S. D.; Ito, O. Bionano donor–acceptor hybrids of porphyrin, ssDNA, and semiconductive single-wall carbon nanotubes for electron transfer via porphyrin excitation. *J. Am. Chem. Soc.* **2011***, 133*, 19922.

26. Wieland, S.; El Yumin, A. A.; Gotthardt, J. M.; Zaumseil, J. Impact of dielectric environment on trion emission from single-walled carbon nanotube networks. *J. Phys. Chem. C* **2023***, 127*, 3112.

27. Barrejon, M.; Gobeze, H. B.; Gomez-Escalonilla, M. J.; Fierro, J. L. G.; Zhang, M.; Yudasaka, M.; Iijima, S.; D'Souza, F.; Langa, F.; Ultrafast electron transfer in all-carbon-based SWCNT-C_{60} donor-acceptor nanoensembles connected by poly(phenyleneethynylene) spacers. *Nanoscale* **2016**, *8*, 14716.

28. Ohtani, M.; Fukuzumi, F. Solubilization and photoinduced electron transfer of single-walled carbon nanotubes wrapped with coenzyme Q_{10}. *Chem. Commun*. **2009**, 4997-4999.

29. Kazemi, S.; Jang, Y.; Liyanage, A.; Karr, P. A.; D'Souza, F. A carbon nanotube binding BODIPY-C_{60} nano tweezer: charge stabilization through sequential electron transfer. *Angew. Chem. Int. Ed.* **2022***, 61,* e202212474.

30. Loudet, A.; Burgess, K. BODIPY dyes and their derivatives: syntheses and spectroscopic properties. *Chem. Rev.* **2007***, 107*, 4891.

31. El-khouly, M. E.; Fukuzumi, S.; D'Souza, F. Photosynthetic antenna–reaction center mimicry by using boron dipyrromethene sensitizers. *ChemPhysChem* **2014***, 15*, 30.

32. Shao, S.; Thomas, M. B.; Park, K. H.; Mahaffey, Z.; Kim, D.; D'Souza, F. Sequential energy transfer followed by electron transfer in a BODIPY–bisstyrylBODIPY bound to C_{60} triad via a 'two-point' binding strategy. *Chem. Commun.* **2018***, 54*, 54.

33. Zarrabi, N.; Obondi, C. O.; Lim, G. N.; Seetharaman, S.; Boe, B. G.; D'Souza, F.; Poddutoori, P. K. Charge-separation in panchromatic, vertically positioned bis(donor styryl)BODIPY–aluminum(III) porphyrin–fullerene supramolecular triads. *Nanoscale* **2018***, 10*, 20723.

34. Sekaran, B.; Guragain, M.; Misra, R.; D'Souza, F. β-pyrrole functionalized push or pull porphyrins: excited charge transfer promoted singlet oxygen generation. *J. Phys. Chem. A* **2023***, 127*, 7964.

35. Lakowicz, J. R. *Principles of fluorescence spectroscopy*, 3rd ed. Springer, Singapore, 2006.

36. Tanaka, Y.; Hirana, Y.; Niidome, Y.; Kato, K.; Saito, S.; Nakashima, N. Experimentally determined redox potentials of individual (n,m) single-walled carbon nanotubes. *Angew. Chem. Int. Ed.* **2009***, 48*, 7655.

37. *Gaussian 16*, Revision A.03, M. J. Frisch, G. W. Trucks, H. B. Schlegel, G. E. Scuseria, M. A. Robb, J. R. Cheeseman, G. Scalmani, V. Barone, G. A. Petersson, H. Nakatsuji, X. Li, M. Caricato, A. V. Marenich, J. Bloino, B. G. Janesko, R. Gomperts, B. Mennucci, H. P. Hratchian, J. V. Ortiz, A. F. Izmaylov, J. L. Sonnenberg, D. Williams-Young, F. Ding, F. Lipparini, F. Egidi, J. Goings, B. Peng, A. Petrone, T. Henderson, D. Ranasinghe, V. G. Zakrzewski, J. Gao, N. Rega, G. Zheng, W. Liang, M. Hada, M. Ehara, K. Toyota, R. Fukuda, J. Hasegawa, M. Ishida, T. Nakajima, Y. Honda, O. Kitao, H. Nakai, T. Vreven, K. Throssell, J. A. Montgomery, Jr., J. E. Peralta, F. Ogliaro, M. J. Bearpark, J. J. Heyd, E. N. Brothers, K. N. Kudin, V. N. Staroverov, T. A. Keith, R. Kobayashi, J. Normand, K. Raghavachari, A. P. Rendell, J. C. Burant, S. S. Iyengar, J. Tomasi, M. Cossi, J. M. Millam, M. Klene, C. Adamo, R. Cammi, J. W. Ochterski, R. L. Martin, K. Morokuma, O. Farkas, J. B. Foresman, and D. J. Fox, Gaussian, Inc., Wallingford CT, 2016.

38. *GaussView*, Version 6.0.16, Roy Dennington, Todd A. Keith, and John M. Millam, Semichem Inc., Shawnee Mission, KS, 2016.

39. Dresselhaus, M. S.; Dresselhaus, G.; Jorio, A.; Souza Filho, A. G.; Saito, R. Raman spectroscopy on isolated single wall carbon nanotubes. *Carbon* **2002**, *40*, 2043.

40. Arellano L. M.; Martin-Gomis, L.; Gobeze, H. B.; Molina, D.; Hermosa, C.; Gomez-Escalonilla, M. J.; Fierro, J. L. G.; Sastre-Santos, A.; D'Souza, F.; Langa, F. Edge-on and face-on functionalized pc on enriched semiconducting SWCNT hybrids. *Nanoscale*, **2018**, *10*, 5205.

41. Rehm, D.; Weller, A. Kinetics of fluorescence quenching by electron and H-atom transfer. *Israel J. Chem.* 1**970**, *8*, 259.

42. Cogdell, R.; Mullineaux, C. Photosynthetic light harvesting - introduction. *Photosynth Res* **2008***, 95*, 117.

43. Shao, S.; Gobeze, H. B.; Karr, P. A.; D'Souza, F. 'Two-point' self-assembly and photoinduced electron transfer in meso-donor-carrying bis(styryl crown ether)-BODIPY-bis(alkylammonium)fullerene donor-acceptor conjugates, *Chem. Asian, J*. **2017**, *12*, 2258-2270.

44. Snellenburg, J. J.; Laptenok, S.; Seger, R.; Mullen, K. M.; van Stokkum, I. H. M. Glotaran: A Java-Based Graphical User Interface for the R Package TIMP. *J. Stat. Softw.* **2012***, 49*, 1.

45. Glotaran, http://glotaran.org/ (site accessed on April 1, 2024).

Table of contents